Journal of Sound and Vibration (1997) **201**(4), 491–513

VIBRATIONAL ENERGY FLOW ANALYSIS USING A SUBSTRUCTURE APPROACH: THE APPLICATION OF RECEPTANCE THEORY TO FEA AND SEA

K. SHANKAR

Department of Engineering Science, University of Oxford, Parks Road, Oxford, OX1 3PJ,

AND

A. J. KEANE

Department of Mechanical Engineering, University of Southampton, Highfield, Southampton, SO17 1BJ, England

(*Received* 18 *March* 1996, *and in final form* 20 *September* 1996)

A method for studying the vibrational energy flows through structures based on receptance theory is presented. The structures are considered to be made up of subsystems, which may, in turn, be substructures modelled by using finite element analysis (FEA), each having been separately analyzed for its eigenvalues and eigenvectors. The method may be classified as a form of substructuring using free–free interface conditions. It differs significantly from traditional substructuring in its use of matrices composed of the substructure Green functions, evaluated as summations over their uncoupled modes, to obtain the displacement contributions of the external and boundary coupling forces; also, the method can readily take into account variations in substructure damping. The proposed method additionally calculates the time averaged substructure vibrational energy levels by evaluating the balance between input and dissipated energies and the energy transfers through coupling nodes. It is therefore of particular interest when using FEA substructures to carry out statistical energy analysis (SEA) studies, since the resulting energy data can be readily applied to evaluate SEA parameters such as coupling loss factors.

The formulation developed has been implemented as a computer program which uses substructure modal information from a commercial FEA package and then combines this to predict the response of the global model. Two simple examples involving two- and three-dimensional FEA models built from beam elements are presented, which show that there is good agreement between the substructure based predictions and the equivalent global models. Moreover, the method presented is computationally more efficient than using global FEA models, even when all the substructure modes are used. The method is then applied to study the SEA coupling loss factors of two further example structures: first, two thin plates joined along an edge at right angles are examined; and then a second, more complicated structure formed from a section of a large marine vessel is studied. The approach is shown to be applicable to any general finite element model which is considered as an SEA subsystem.

1. INTRODUCTION

A formulation for predicting the energy levels of a general structure, based on the modal properties of uncoupled substructures, is presented. Such subsystem-wise predictions of energy levels for complex structures are of interest in acoustics and related fields, especially Statistical Energy Analysis (SEA) [1]. In SEA, estimation of the so called "coupling loss

0022–460X/97/140491 + 23 $25.00/0/sv960769

factors'' applying between various substructures (or subsystems in SEA terminology) is crucial to the prediction of high frequency vibrational energy levels. The data usually required to evaluate these factors, either by experimental or numerical means, are the powers input to the subsystems and the resulting, time averaged, energy levels. These are also commonly averaged spatially over a number of forcing and response points and/or across a range of frequencies. The substructure method proposed here is primarily intended to provide such data from FEA models and also, in a reverse sense to check the reliability of SEA predictions for given structures. A fundamental feature of the approach (and other substructuring methods) is the desire for much higher frequencies to be made accessible from FEA models than would be achieved if global FEA models of the combined subsystems were used instead.

A formulation for predicting the energy flows through rigidly coupled beam networks by using receptance theory has been recently presented by the authors [2]. In that study, the behaviour of a global structure of beams was predicted from the Green functions of the uncoupled elements: i.e., matrices of Green functions were used to derive expressions for the beam-end displacements in the form of the contributions of the external driving and unknown boundary coupling forces. Enforcement of suitable boundary conditions at the beam-ends was used in the formation of a number of complex simultaneous linear equations with the boundary coupling forces as the unknowns; once these are solved, it is possible to find the energy flows through the various substructures. In the present work this formulation has been extended to discrete models. The main differences between the two approaches are: (a) the use of FEA derived mode shapes instead of analytical ones (note that the numerically derived FEA mode shapes used constitute a finite set of orthogonal modes, as against the analytically derived, infinite set of orthogonal modes used in the previous work—this has implications for the convergence of the Green function modal summations); (b) the present formulation has to consider substructure coupling at an arbitrary number of joints per substructure and hence it is set up to deal with many cross receptances; and (c) the need to use any general substructure makes is necessary to assume modal coupling between **x**, **y** and **z** displacements and rotations at any point.

Receptance theory provides a method for predicting the behaviour of a composite system based on a proper combination of the component receptances [3]. One of the advantages of the receptance approach is its ability to calculate directly substructure energy transfers, since it deals in both the junction forces and displacements; it can also allow for substructure specific damping. This is not to say that approaches such as the dynamic stiffness method (or indeed other substructuring approaches) cannot yield interface forces; rather, that the receptance method is perhaps the most natural approach to adopt when interface forces are required. Receptance methods have therefore often been applied to SEA, which deals with the energy flows in systems of coupled substructures (subsystems in SEA terminology) under conditions such as random external forcing, weak coupling strengths and high modal density. Such work has often been focused on the validity of the assumptions underlying SEA by the deterministic study of energy flows through simple systems of coupled beams or rods; see, for example, the papers of Davies [4], Remington and Manning [5], Clarkson [6] and Keane and Price [7]. The approach can, however, be somewhat less computationally efficient than some of the alternatives when dealing with problems with large numbers of coupling points. Here it is applied to SEA studies in which FEA has been used to analyze individual subsystems. Such analyses usually involve relatively few interface points and so such inefficiencies are rarely a significant problem, especially given the direct availability of the coupling forces which are needed in SEA. Moreover, as is demonstrated later, the approach is still significantly faster than global FEA, in which all of the modes of a structure must be dealt with.

Finally, it should be noted that FEA models have recently been used by a number of other workers to evaluate SEA coupling loss factors or study the validity of the many assumptions inherent in SEA; for example, by Nefske and Sung [8], Wood [9], Hambric [10], Steel and Craik [11], Simmons [12] and Fredo [13]. The formulation proposed in this paper is aimed at reducing some of the shortcomings found by these various workers, by increasing the range of frequencies considered while producing exact energy balances and enabling the use of damping levels which differ from subsystem to subsystem.

2. FORMULATION

As has already been noted, the authors have recently presented a receptance based approach for studying the behaviour of coupled, two-dimensional substructures [2]. The extension of this work to deal with arbitrary numbers of coupling points per (three-dimensional) substructure and the finite sets of modes resulting from FEA, as opposed to classical calculations, is relatively straightforward. In this case, the external forcing vector on a substructure (A), due to loading at point $\hat{I}e$, $\{\mathbf{F}_{(A)}\}^{\hat{I}e}$, is constituted by six component forces corresponding to the local $\mathbf{x}$, $\mathbf{y}$, $\mathbf{z}$, θ_x, θ_y and θ_z co-ordinates: i.e., $\mathbf{F}^{\hat{I}e}_{(A).x}$, $\mathbf{F}^{\hat{I}e}_{(A).y}$, $\mathbf{F}^{\hat{I}e}_{(A).z}$, $\mathbf{F}^{\hat{I}e}_{(A).\theta.x}$, $\mathbf{F}^{\hat{I}e}_{(A).\theta.y}$ and $\mathbf{F}^{\hat{I}e}_{(A).\theta.z}$. The coupling force vectors at the I, J, K, . . . coupling points of each substructure, such as $\{\mathbf{F}_{(A)}\}^I$, $\{\mathbf{F}_{(A)}\}^J$, $\{\mathbf{F}_{(A)}\}^K$ . . . , are likewise each constituted by six component forces, represented in similar notation.

The expression for a six-dimensional local displacement vector, such as $\{\mathbf{x}_{(A)}\}^I$, may then be represented by

$$\sum_{\hat{N}=\hat{I}}^{\hat{Z}} [\mathbf{G}_{(A)}]^{I\hat{N}e}\{\mathbf{F}_{(A)}\}^{\hat{N}e} + \sum_{N=I}^{Z} [\mathbf{G}_{(A)}]^{IN}\{\mathbf{F}_{(A)}\}^{N} = \{\mathbf{x}_{(A)}\}^I, \tag{1}$$

where all the matrices of Green functions for the substructure (A), $[\mathbf{G}_{(A)}]$, are of order 6×6, e.g.,

$$[\mathbf{G}_{(A)}]^{IJ} =$$

$$\begin{bmatrix}
\mathbf{G}_{(A)}(I.x,J.x) & \mathbf{G}_{(A)}(I.x,J.y) & \mathbf{G}_{(A)}(I.x,J.z) & \mathbf{G}_{(A)}(I.x,J.\theta_x) & \mathbf{G}_{(A)}(I.x,J.\theta_y) & \mathbf{G}_{(A)}(I.x,J.\theta_z) \\
\mathbf{G}_{(A)}(I.y,J.x) & \mathbf{G}_{(A)}(I.y,J.y) & \mathbf{G}_{(A)}(I.y,J.z) & \mathbf{G}_{(A)}(I.y,J.\theta_x) & \mathbf{G}_{(A)}(I.y,J.\theta_y) & \mathbf{G}_{(A)}(I.y,J.\theta_z) \\
\mathbf{G}_{(A)}(I.z,J.x) & \mathbf{G}_{(A)}(I.z,J.y) & \mathbf{G}_{(A)}(I.z,J.z) & \mathbf{G}_{(A)}(I.z,J.\theta_x) & \mathbf{G}_{(A)}(I.z,J.\theta_y) & \mathbf{G}_{(A)}(I.z,J.\theta_z) \\
\mathbf{G}_{(A)}(I.\theta_x,J.x) & \mathbf{G}_{(A)}(I.\theta_x,J.y) & \mathbf{G}_{(A)}(I.\theta_x,J.z) & \mathbf{G}_{(A)}(I.\theta_x,J.\theta_x) & \mathbf{G}_{(A)}(I.\theta_x,J.\theta_y) & \mathbf{G}_{(A)}(I.\theta_x,J.\theta_z) \\
\mathbf{G}_{(A)}(I.\theta_y,J.x) & \mathbf{G}_{(A)}(I.\theta_y,J.y) & \mathbf{G}_{(A)}(I.\theta_y,J.z) & \mathbf{G}_{(A)}(I.\theta_y,J.\theta_x) & \mathbf{G}_{(A)}(I.\theta_y,J.\theta_y) & \mathbf{G}_{(A)}(I.\theta_y,J.\theta_z) \\
\mathbf{G}_{(A)}(I.\theta_z,J.x) & \mathbf{G}_{(A)}(I.\theta_z,J.y) & \mathbf{G}_{(A)}(I.\theta_z,J.z) & \mathbf{G}_{(A)}(I.\theta_z,J.\theta_x) & \mathbf{G}_{(A)}(I.\theta_z,J.\theta_y) & \mathbf{G}_{(A)}(I.\theta_z,J.\theta_z)
\end{bmatrix}$$

$$= [[\mathbf{G}_{(A)}]^{JI}]^{\mathrm{T}}. \tag{2}$$

The Green functions take the traditional form of sums over modes, but are now calculated from the finite orthogonal sets of modes generated by the FEA solutions for the individual substructures, with the interface between the substructures set free. For example, the x component response at I due to y component forcing at J is

$$\mathbf{G}(I.x, J.y) = \sum_{r=0}^{n} \frac{\phi^I_{r.x}\phi^J_{r.y}}{M_r\Delta_r}, \tag{3}$$

where $\phi^I_{r.x}$ is the xth component of the rth mode shape at point I, $\Delta_r = \omega_r^2 - \omega^2 + \mathrm{i}c\omega$, ω_r is the rth natural frequency and c, the ratio of damping coefficient to mass of the substructure, such that the damping ratio, ζ, is given by $c = 2\zeta\omega_r$. Here the n modes of the substructure are normalized to have unit modal masses, i.e.,

$$[\bar{\mathbf{\Phi}}]^{\mathrm{T}}[\mathbf{M}][\bar{\mathbf{\Phi}}] = [\mathbf{I}], \tag{4}$$

where the normalized modal matrix $[\bar{\mathbf{\Phi}}]$ is obtained by dividing the rth column of $[\mathbf{\Phi}]$ by the square root of the modal mass M_r. Such a scheme can be helpful for assigning modal damping, since the separate modal masses then need not be taken into account, making it easier to assign damping parameters relative to other substructures: this is particularly useful for assigning constant coefficient damping. Adoption of the mass normalized mode shapes $[\bar{\mathbf{\Phi}}]$ simplifies the equation for the Green function summation to

$$\mathbf{G}(I.x, J.y) = \sum_{r=0}^{n} \frac{\bar{\phi}^I_{r.x}\bar{\phi}^J_{r.y}}{\Delta_r}. \tag{5}$$

For free–free substructures, six rigid body modes have to be included in these modal summations, consisting of three purely translatory modes and three purely rotary modes, or six linear combinations involving them. These are evaluated in most FEA packages along with the flexible modes and can be readily included in the summations, with the corresponding natural frequencies set to zero.

The scheme for the assembly of equations, solution of the joint coupling forces and power calculations, once they have been transformed into a consistent global co-ordinate scheme, is relatively straightforward and as per the previous reference [2]. Since the coupling force vectors are constituted by six components here, the order of the complex matrix solution becomes six times the total number of coupling points on all the substructures. It should also be recalled that, when using FEA models in SEA, it is often necessary to average results over a number of different forcing points. The responses to multiple forcing at different points on a substructure are obtained here by summing up the external forcing contribution matrices on the right sides of the equations. Therefore, when the responses due to separate forcing at different points are required, the final form of the assembled matrix equations allows schemes such as Crout factorization to be applied, which permit multiple right sides to be solved with little extra computational effort once the decomposition and triangularisation of the left side has been carried out. This allows the almost simultaneous evaluation of subsystem energies for the different cases of external forcing being considered.

To carry out the substructuring process the separate subsystems are solved for their eigenvalues and vectors, which are then used by the receptance formulation to predict the displacements and forces at the coupling joints. These then allow the direct calculation of the various energy flows through the couplings and hence the energy dissipations within each substructure. The various energy levels are then obtained from these dissipated powers using the damping coefficients. To check the validity of the calculations the displacements may be compared against those from a global FEA model, obtained by merging the subsystems without any alteration of the mesh properties. Also, the power input to the system can be verified to be equal to the sum of the dissipated powers of all the substructures.

Here, all the finite element calculations have been performed by using the IDEAS-VI package [14], which has both similarity transformation and iterative eigenvalue solvers. The former reduces the system matrix to diagonal form through matrix rotations and can

be used to extract the complete set of modes for small models. The Householder-QL and Jacobi methods are of this type, the former being faster as it performs all the operations in core (which also restricts the size of the model), whereas the latter writes the intermediate data to disk, making it suitable for the solution of larger models. The iterative method, which uses the Simultaneous Vector Iteration (SVI) algorithm, is suitable for very large models, although only a limited number of modes can be extracted at one time.

In some of the examples given below, the CPU times taken for the extraction of global modes are compared with those when using the receptance approach over the entire set of substructure eigenvalues. It may be noted that it is often not feasible to extract the entire set of substructure eigenvalues for large models, and if such a need occurs then other direct methods of dynamic matrix inversion must be used. However, the intention here is to demonstrate that even if only a proportion of the substructure modes are used, the advantages over using a few global modes are still appreciable; in this case the numerical accuracy of the energy balance must be checked to ensure that errors due to modal truncation are acceptable. It should also be recalled that some other substructuring approaches, such as the dynamic stiffness method, would probably be as fast or faster in solving for displacements as the method proposed here. Such methods are, however, not yet widely available; the general purpose FEA code used here, for example, does not include such approaches [14].

The time required for processing the substructure data when using the receptance formulation depends on the number of driving frequencies at which the energy levels or displacements are to be evaluated, each requiring the evaluation of the Green functions and the solution of a set of complex equations, the order of which is dependent on the number of coupling points. It may be noted that the matrix size is independent of the number of substructure modes used in the summation, which makes it feasible to include all the substructure modes in the calculation if they are available. The evaluation of the Green functions is made easier by the use of (a) stored FEA derived mode shapes and frequencies and (b) the matrix transpose relations between the coupling points, such as $[\mathbf{G}_{(A)}]^{MN} = [[\mathbf{G}_{(A)}]^{NM}]^{\mathrm{T}}$. The computational effort involved in the assembly and solution of these equations is more than offset, for large structures, by the fact that the modes used are obtained by solving subsystems of reduced size. It also allows the various energy flows to be calculated directly with negligible further effort.

3. INITIAL EXAMPLES

After having outlined the approach to be adopted, and before going on to perform SEA calculations, two simple beam based examples are presented next to illustrate the substructuring process. The structures analyzed are illustrated in Figures 1 and 2. They have both been modelled with the IDEAS-VI finite element package by using linear beam elements and subjected to unit point harmonic forcing of the type $\mathbf{F} = \mathrm{Re}\{1\, \mathrm{e}^{\mathrm{i}\omega t}\}$. The beams were taken to have the following properties: second moments of area, $I_{yy} = I_{zz} = 1 \times 10^{-7}\,\mathrm{m}^4$, cross-sectional area, $A_{xx} = 3{\cdot}49 \times 10^{-4}\,\mathrm{m}^2$, modulus of elasticity, $E = 2 \times 10^{11}\,\mathrm{N\,m}^{-2}$, density, $\rho = 7851\,\mathrm{kg\,m}^{-3}$ and Poisson ratio, $v = 0{\cdot}3$.

3.1. EXAMPLE 1

The first example consists of two plane substructures, being discretized with 246 and 252 d.o.f., respectively, the latter having, in addition, three rigid body modes. The combined FEA model, obtaining by merging nodes at the coupling joints J_1 and J_2, has 492 d.o.f., which yield 492 flexible modes. The undamped substructure modes, after extraction, were normalized for unit modal masses. The ratio of damping coefficient to

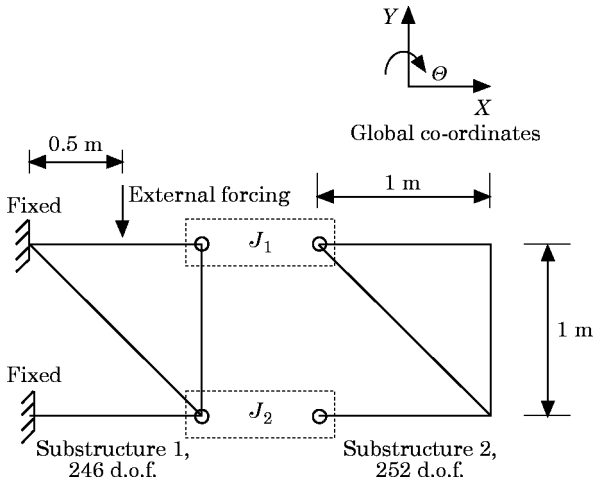

Figure 1. Example 1, a two-dimensional, two-substructure model.

mass for both substructures was set to 100·0 in the receptance formulation. The undamped global modes were similarly normalized and all modes assigned a damping coefficient of 100·0, which correctly simulates the substructure damping. The complete set of modes were extracted in double precision for the two substructures and for the global model. The solution time requirements were as shown in Table 1.

The additional time required to combine the two substructures, when using the receptance formulation, was 250 CPU seconds for the 500 frequencies considered within the frequency domain of 0–5000 Hz each frequency step requiring the assembly and solution of a complex 12×12 matrix. Even after taking into account such overheads, the saving in time due to the substructure approach proposed is quite significant. The **X**, **Y** and Θ displacements at J_2, obtained from the receptance formulation and the FEA global

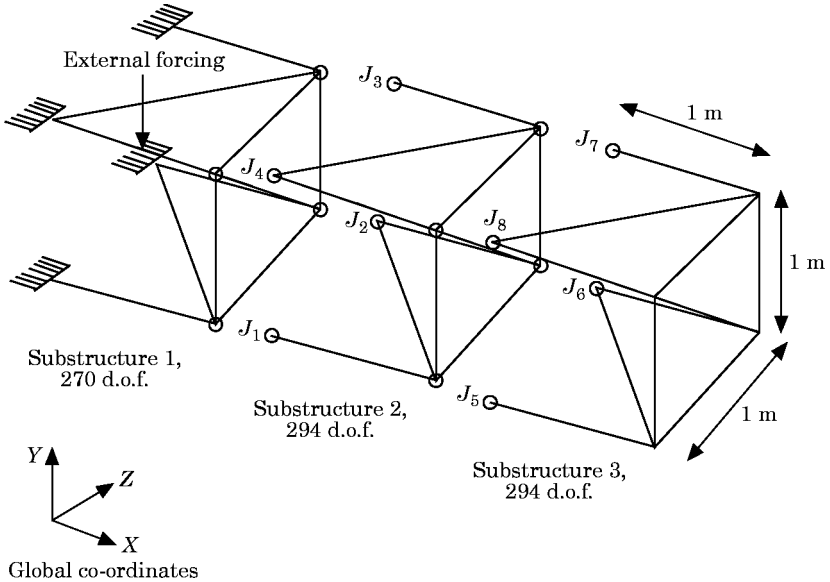

Figure 2. Example 2, a three-dimensional, three-substructure model.

TABLE 1

Time required for solution (*CPU seconds*), *Example* 1

Solution method	Substructure 1	Substructure 2	Global model
Householder-QL	73	78	Not solved
Jacobian	225	240	2880

models are compared in Figure 3; the curves are essentially superimposed, showing that the two methods produce identical results. Although only the range 0–5000 Hz is shown in the figure, it is found that inclusion of the entire set of substructure modes gives accurate results throughout the eigenvalue frequency range.

The inclusion of sufficient substructure modes being important to the accuracy of the receptance based prediction, in Figures 4 and 5 are shown the effects of taking into account 25%, 50%, 75%, 90% and 100% of these substructure modes when calculating the energy levels of substructures 1 and 2. The severity of the influence of substructure modal truncation clearly varies with frequency, and only a detailed study of the modal participation factors at the driving and response points can give insight into the modal contributions for any particular driving and response configuration. Frequency band averaging is one method that can be used to minimize the effect of such errors; its efficacy, however, depends on the modal density and overlap factors of the system. In Figures 6(a) and (b) are shown the effect of frequency averaging, with bandwidths of 100 Hz and 200 Hz for the energy levels of substructure 1 (cf., Figure 4). The percentage variations from the exact case are shown and it is clear that the errors arising when using a 200 Hz

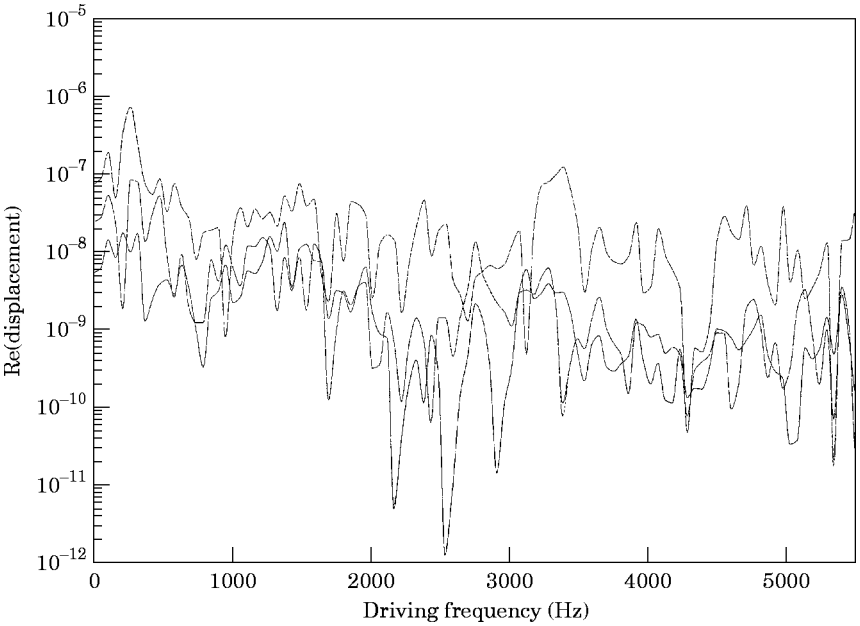

Figure 3. Example 1: displacements at J_2 calculated via substructure and global FEA models (results almost superimposed). ———, X displacement, substructure calculation; - - - - -, Y displacement, substructure calculation; –·····–·····–, Θ displacement, substructure calculation; – – –, X displacement, global FEA calculation; –···–···–, Y displacement, global FEA calculation;

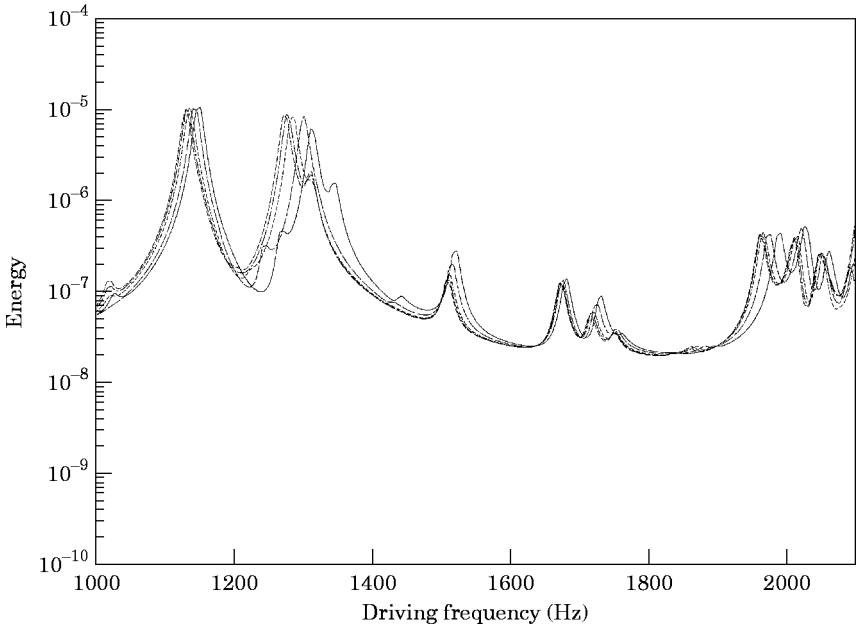

Figure 4. Example 1: variations in substructure 1 energy levels for variations in the number of substructure modes. ———, 25% of modes; - - - - -, 50% of modes; –·–·–·–·–, 90% of modes; – – –, all modes.

bandwidth are much less than for a 100 Hz bandwidth, as might be expected, although more detail is lost from the results.

It is also worth examining the behaviour of the Green functions with respect to the number of modes in the summation being used. In an analytical model, where there are

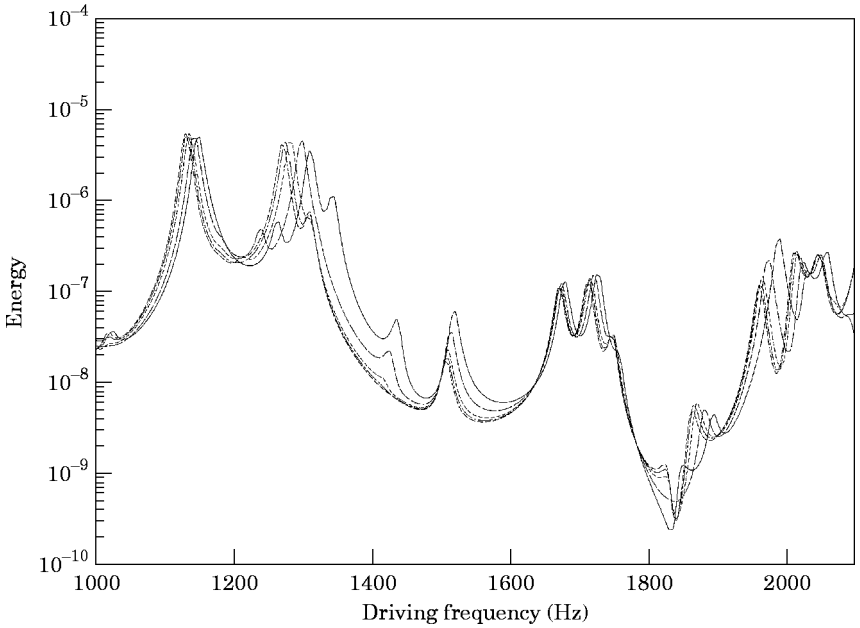

Figure 5. Example 1: variations in substructure 2 energy levels for variations in the number of substructure modes (key as Figure 4).

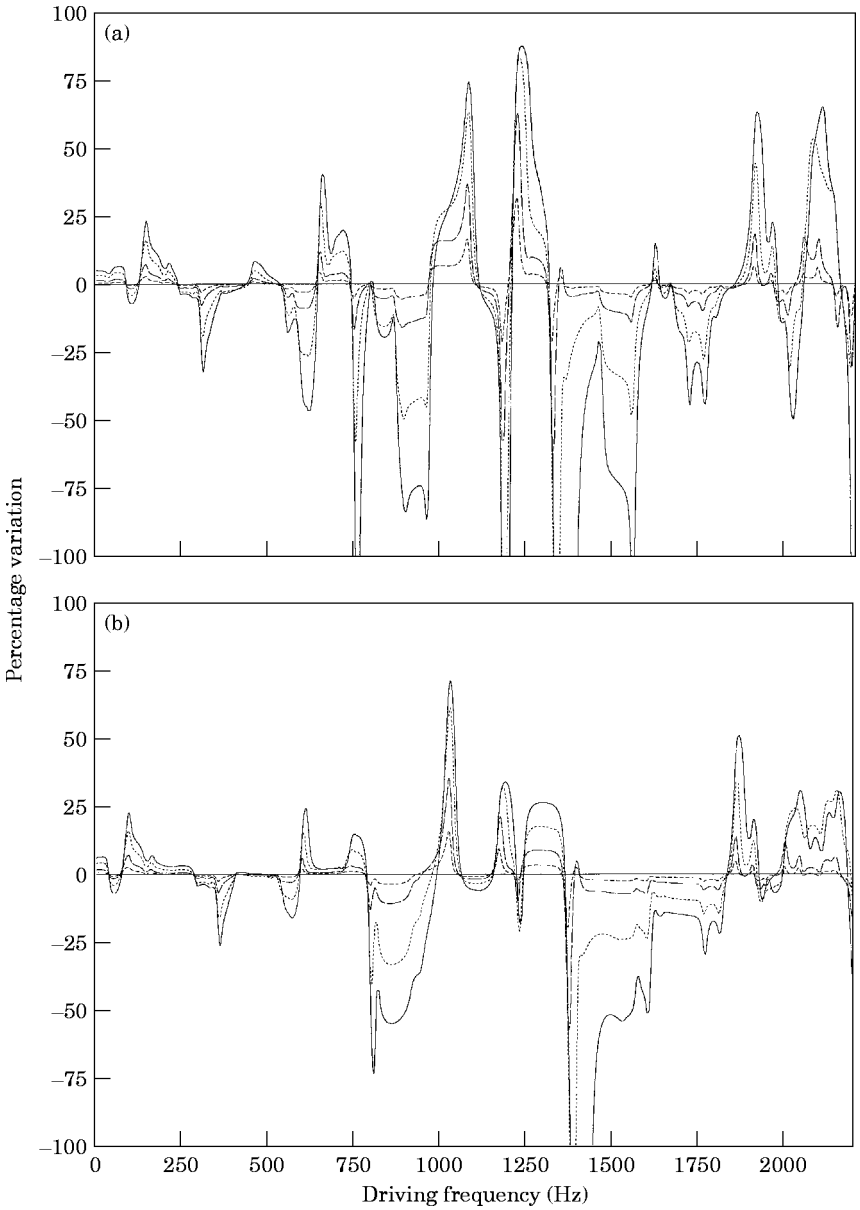

Figure 6. Example 1: variations in the frequency band averaged substructure 1 energy levels for variations in the number of substructure modes, (a) by using a bandwidth of 100 Hz and (b) by using a bandwidth of 200 Hz (key as Figure 4).

an infinite number of orthogonal modes, the inability to include all of the modes leads to problems regarding the convergence of the functions. In discrete FEA models, however, the Green function summation can include the complete finite set of orthogonal modes, giving responses which are exact relative to that model. If the model is coarsely discretized, however, the inclusion of each additional mode in the summation causes a jump in its value, leading to a "staircase" variation in the function. In Figure 7 is shown the Green function of the rotary modes at 1000 Hz for J_2 of substructure 1. The effect of the rather

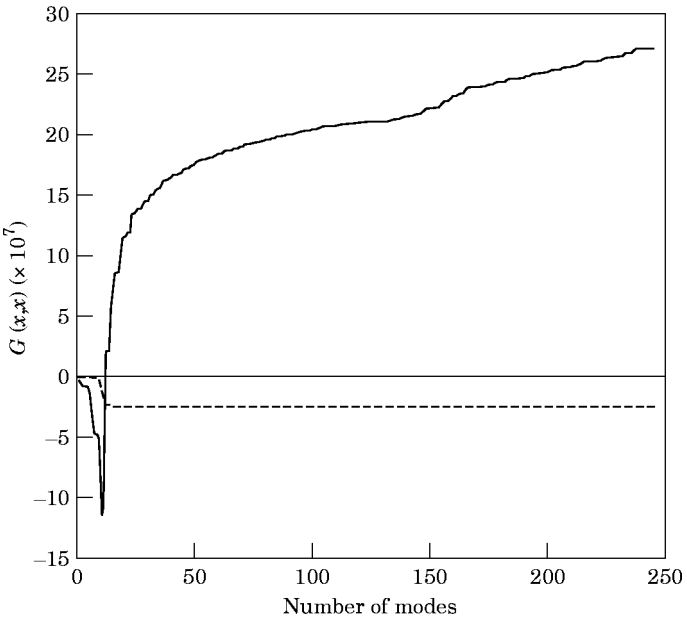

Figure 7. Example 1: convergence of the rotary Green Function at 1000 Hz for substructure 1. ———, Real part; – – – –, imaginary part.

coarse modes involved is clear, although the final summation value (using all 246 modes) is exact relative to the global model.

3.2. EXAMPLE 2

Next, a three-dimensional model consisting of three substructures is studied; again see Figure 2. Here substructure 1 has 270 d.o.f. and is fully fixed at its base points, whereas substructures 2 and 3 have 294 d.o.f. and are free–free, each possessing six rigid body modes in addition to the set of flexible modes. The global structure, obtained by merging the coupling point nodes, has 810 d.o.f. In this example the complete set of eigenvectors for the substructures were readily extracted in double precision. The matrix size of the global model necessitated the use of the iterative solver, and only a limited number of modes were extracted in single precision due to the significant computational effort involved. The solution time requirements were as shown in Table 2.

Since the frequencies of the global model are truncated at the 250th mode, which corresponds to 1770 Hz, a limited frequency domain of 0–2000 Hz is considered for the substructure combination. The time taken to combine the substructure, using the receptance formulation, was 1500 s for the 200 frequencies considered, each frequency step requiring the assembly and solution of a 96×96 complex matrix. While this example again

TABLE 2

Time required for solution (*CPU seconds*), *Example* 2

Solution method	Substructure 1	Substructure 2	Substructure 3	Global model
Householder-QL	200	263	263	Not solved
Jacobian	405	471	471	Not solved
Iterative	—	—	—	3100 (12 iterations, 250 modes)

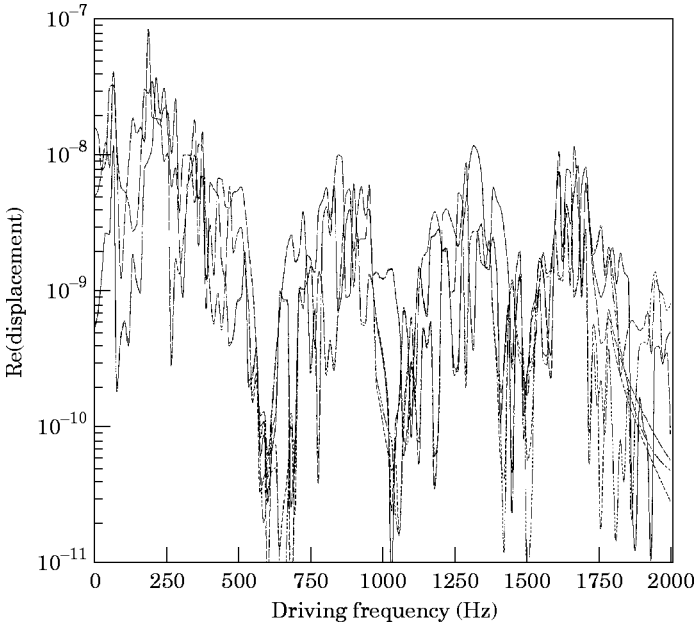

Figure 8. Example 2: translatory displacements at J_6 calculated via substructure and global FEA models. ———, X displacement, substructure calculation; - - - - -, Y displacement, substructure calculation; –·····–·····–, Z displacement, substructure calculation; – – –, X displacement, global FEA calculation; –···–···–, Y displacement, global FEA calculation; ....., Z displacement, global FEA calculation.

shows that there is appreciable saving in time by adopting the receptance formulation, it may be also noted that the method gives accurate results throughout the frequency domain of the combined model, which cannot be obtained by the solution of the equivalent global model unless all its modes are extracted.

The six displacement components of the model at J_6, obtained by the receptance formulation and the global FEA model are compared in Figures 8 (**X**, **Y**) and 9 (Θ_X, Θ_Y and Θ_Z). The curves are in good agreement, especially in the low frequency ranges where they are superimposed on each other; the deterioration of the FEA results near 1770 Hz followed by the abrupt truncation in the responses are clearly shown. Lastly, in Figure 10 are shown the input and dissipated powers in the three substructures due to driving substructure 1, a much larger frequency domain being considered in this case. It is shown in the figure how, over certain portions of the frequency range, the dissipated power of the driven system nearly equals the input power because of the very small losses occurring in the undriven systems for this example.

4. FEA AND SEA

Attention is next focused on how the substructuring approach presented here can be used in energy flow studies of complex structures, and in particular how these may be related to SEA. It will be recalled that SEA is concerned with formulating simple, linear equations that predict the flow of vibrational energy around structures using quantities known as coupling loss factors (CLFs) [1]. Once the CLFs are known, the use of SEA is quite straightforward, although it is far from obvious how accurate a particular SEA model will be in practice, unless a number of rather restrictive assumptions hold [15]. It should be noted at the outset that FEA is an essentially deterministic tool, while SEA is

concerned with average results. Thus, to apply the results of FEA to traditional SEA, some kind of averaging is required. Formally, SEA is concerned with averages over ensembles of similar but not identical systems carried out frequency by frequency. It is, however, commonly applied to averages over frequency on a single system. Either approach can be adopted when using FEA results, although it is usually more convenient to average over frequency for results from a single FEA run, and that is the approach used here. It should be noted, however, that useful results can also be obtained without averaging the FEA results at all, and this approach is also used in the present work. In such circumstances the quantities produced by the approach are then not strictly coupling loss factors at all but, rather, energy flow coefficients; here the term "coupling loss factor" is used throughout to avoid confusion. Lastly, it should be mentioned that it is common practice in SEA to average results over a range of forcing and response points when deducing CLFs, especially when dealing with problems involving radiated noise: this approach is also used here.

The basic approach to using FEA with SEA is to treat the FEA model as a test-bench on which SEA experiments can be conducted, much as they would be for real experiments. Thus power is injected into various parts of the FEA model and the response calculated: these are then used to deduce the parameter values of the SEA model. The data obtained from applying the resulting model for other forcing cases can then be used to check its range of validity. The attraction of using FEA in this way, rather than the semi-infinite subsystem wave analysis of classical SEA, is its ability to work with complex subsystems at low frequencies. Moreover, existing experience of using FEA models for this purpose suggests that only approximate mode shapes are required when predicting frequency averaged energy levels, albeit subject to certain restrictions; this may significantly reduce

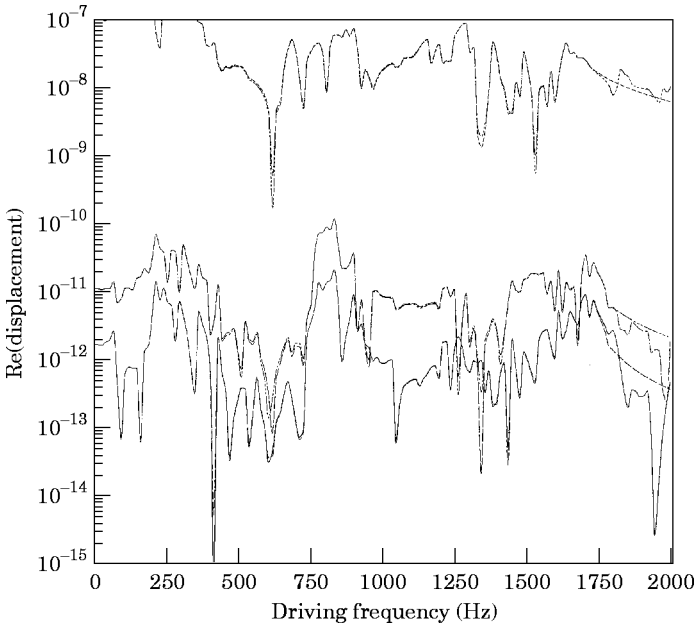

Figure 9. Example 2: rotary displacements at J_6 calculated via substructure and global FEA models. ———, Θ_X displacement, substructure calculation; - - - - -, Θ_Y displacement, substructure calculation; –·····–·····–, Θ_Z displacement, substructure calculation; – – –, Θ_X displacement, global FEA calculation; –···–···–, Θ_Y displacement, global FEA calculation; ....., Θ_Z displacement, global FEA calculation.

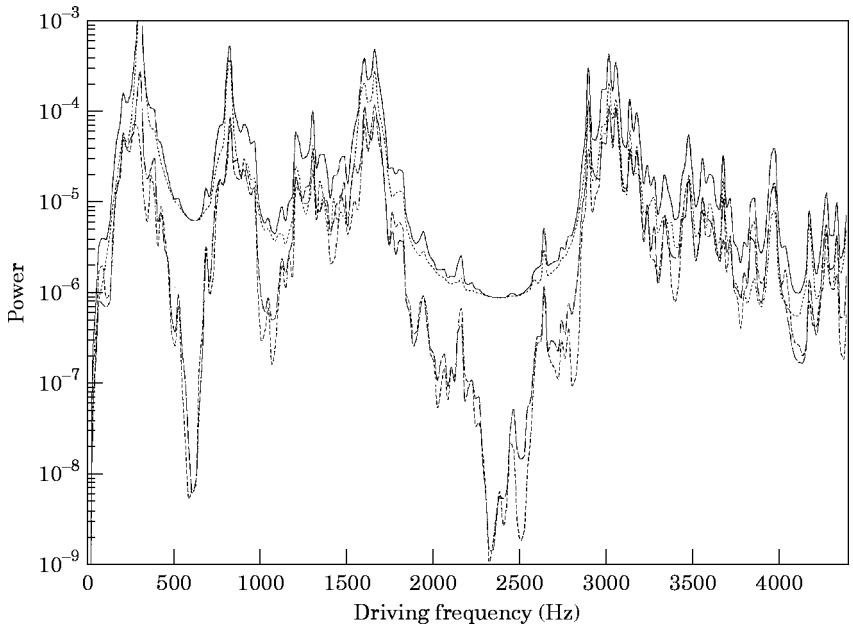

Figure 10. Example 2: input and dissipated powers. ———, input power;....., substructure 1 dissipated power; - - - - -, substructure 2 dissipated power;– – –, substructure 3 dissipated power.

the computational burden associated with finite element models (which is a prime source of criticism of the approach) and thus extend its useful frequency range to higher limits.

The literature describing the existing methods of using FEA models for energy flow studies, cited in the introduction, suggests certain improvements which could enhance its effectiveness for SEA work. Those addressed here are as follows. (a) The present tendency is to use global FEA models of the combined subsystems, which leads to significantly greater computational burdens and lower frequency ranges. (b) Using global modes makes it difficult to apply separate internal damping levels to the various subsystems (most FEA packages currently allow only damping of the global modes, with a common damping factor for the combined subsystems). (c) The normal procedure for finding subsystem energy levels is to square the nodal velocities in each subsystem and multiply them by the values of the lumped masses at each node. This method is not only approximate, due to its adoption of lumped, rather than consistent masses, but also tedious since it necessitates careful assignment of the node numbers so as to be able to decide which subsystem each node belongs to. While this may be accomplished in smaller models, it is difficult to implement in complex structures without a great deal of human interaction. (d) The procedure for finding energies averaged over a range of forcing points is also tedious, since the energy levels due to excitation at different locations have to be separately evaluated and then averaged. As has already been noted, the receptance based subsystem formulation adopted here overcomes most of these shortcomings. However, care must be taken in using the results of such studies: here the aim is not to deduce coupling loss factors *per se*. Rather, the idea is to illustrate some of the likely difficulties that would be encountered in using SEA on models of the type analyzed. For instance, the examples studied highlight the effects of so called "indirect" CLFs which allow for energy exchanges between subsystems not directly coupled to each other and which lie outside the framework of classical SEA. Additionally, some of the CLFs found become negative at times, which is not possible in

the normal use of SEA; here it shows where a traditional use of SEA would be liable to give difficulties.

5. SEA CALCULATIONS

To illustrate the receptance based approach proposed, two further examples are studied from the viewpoint of SEA coupling loss factors (CLFs). The first is a structure consisting of two thin plates connected at right angles along a common edge which is constrained to have purely rotary motion (see Figure 11). This model was studied by Dimitriadis and Pierce [16] who showed that the energy flows at high modal overlap factors and high frequencies approach SEA predictions based on semi-infinite plates. The plate dimensions and materials used here are the same as in the reference. The last example is a much more complex structure, being a section taken from a Small Waterplane Area Twin Hulled (SWATH) ship, a large marine vessel (see Figure 12). It has a central superstructure and two submerged hulls, placed symmetrially on either side of it. This section is divided into three subsystems, along obvious partition lines, and its direct and indirect CLFs studied using the receptance formulation. Both examples were again modelled using the I-DEAS-VI FEA package [14], with results being averaged across a range of forcing and response points. For these examples the modal solutions were obtained using the SVI solver in the package.

5.1. EXAMPLE 3

The two plates in this example were taken to have the following dimensions and properties: vertical plate (plate 1), $0{\cdot}5334\,\text{m} \times 0{\cdot}4572\,\text{m}$, horizontal plate (plate 2), $0{\cdot}3819\,\text{m} \times 0{\cdot}4572\,\text{m}$, thickness, $t = 0{\cdot}001587\,\text{m}$; modulus of elasticity, $E = 6{\cdot}95 \times 10^{10}\,\text{N m}^{-2}$; density, $\rho = 2790\,\text{kg m}^{-3}$; and Poisson ratio, $\nu = 0{\cdot}33$. The wave speed of such plates is given by $c_L = [E/\rho(1 - \nu^2)]^{1/2}$ [16], which gives a value of $5287\,\text{m}^{-1}\,\text{s}$ in this case. The finite element model used here for the plate 1 had 340 quadrilateral thin shell elements and that of plate 2, 238 elements, all having an approximately unit aspect ratio. The resulting element dimensions are typically 0·025 m square, and this satisfies the condition of being less than a third of the bending wavelength, even at high frequencies.

For plate 1, 280 mode shapes (including one rigid body mode) were extracted, spanning the frequency range up to 7500 Hz; for the smaller plate, with rather lower modal density, 190 modes were extracted, spanning the same range. The eigenvalues were extracted to an accuracy of four digits and this took approximately 30 minutes CPU time for each plate. The model had 18 interface nodes along the common edge, each having only a single rotary degree of freedom; hence the order of the assembled complex receptance matrix to be solved at each frequency was 36×36. Frequencies of up to 4000 Hz were studied for CLFs, although values up to 5500 Hz yielded consistent energy balances: i.e., the input powers matched the sum of the subsystem dissipated powers. Beyond that the values were not reliable for use in the CLF equations. All the subsystem modes were mass normalized to unity and then given damping coefficients. An equivalent global model of the two plates was created by merging the interface nodes to measure the time taken to solve for the global modes; the extraction of 60 eigenvalues, to three-digit accuracy, exceeded two and a half hours CPU time and these frequencies spanned less than 1000 Hz in this case. This significantly increased solution time clearly demonstrates the advantage of using a substructure approach to extend the upper limit of the frequency ranges being studied.

In Figure 13 is illustrated the SEA model used in this example, showing the CLFs, for the two plates, here referred to as subsystems 1 and 2. To calculate the CLFs the power injection method is used: in this method, power is first injected into subsystem 1, keeping

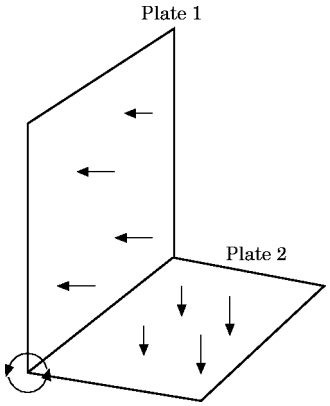

Figure 11. Example 3: two plates coupled along a common, simply supported edge.

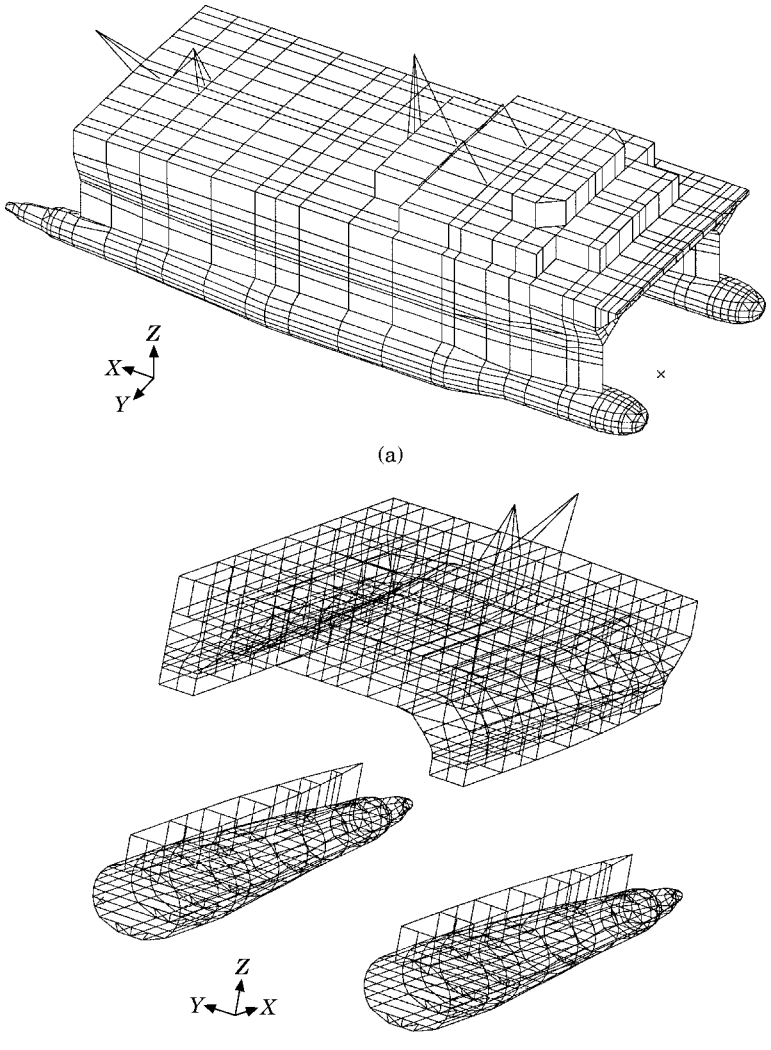

Figure 12. Example 4: FEA meashes of the SWATH ship. (a) Whole ship; (b) aft section broken into subsystems.

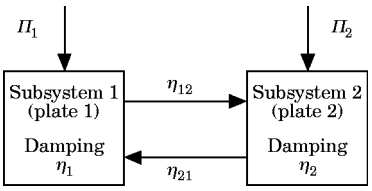

Figure 13. The subsystem model for the two plates of Example 3 showing SEA parameters.

subsystem 2 undriven (case A) and then subsystem 2 is forced with subsystem 1 undriven (case B). Starting with case A, 20 nodes were selected at random on subsystem 1, with a uniform spatial distribution, and each externally forced to find the time averaged energy levels (which may be calculated simultaneously, as noted earlier). These were then averaged together to give the mean input power to subsystem 1 (Π_{1A}) and the mean energies of subsystems 1 and 2 (E_{1A} and E_{2A}). Likewise, for case B, subsystem 2 alone was forced and Π_{2B}, E_{1B} and E_{2B} obtained in similar fashion. The following set of equations are then used to calculate the CLFs, η_{12} and η_{21}. Note that, the internal damping ratios η_1 and η_2 are given, but in these equations they are treated as unknowns and their recalculated values then serve as a check on the accuracy of the derived CLFs:

$$\Pi_{1A}/\omega = \eta_1 E_{1A} + \eta_{12} E_{1A} - \eta_{21} E_{2A}, \qquad 0 = \eta_2 E_{2A} - \eta_{12} E_{1A} + \eta_{21} E_{2A}, \tag{6, 7}$$

$$\Pi_{2B}/\omega = \eta_2 E_{2B} - \eta_{12} E_{1B} + \eta_{21} E_{2B}, \qquad 0 = \eta_1 E_{1B} + \eta_{12} E_{1B} - \eta_{21} E_{2B}. \tag{8, 9}$$

After having obtained the CLFs from these equations, the effects of variation in modal overlap factor (MOF) on the apparent modal density ratio may be examined. According to traditional SEA theory this ratio should be given by η_{12}/η_{21}, and if this lies far from the actual modal density it indicates that the basic SEA assumptions are no longer valid. Here the asymptotic value of the ratio should be 0·716, i.e., the ratio of the plate areas;

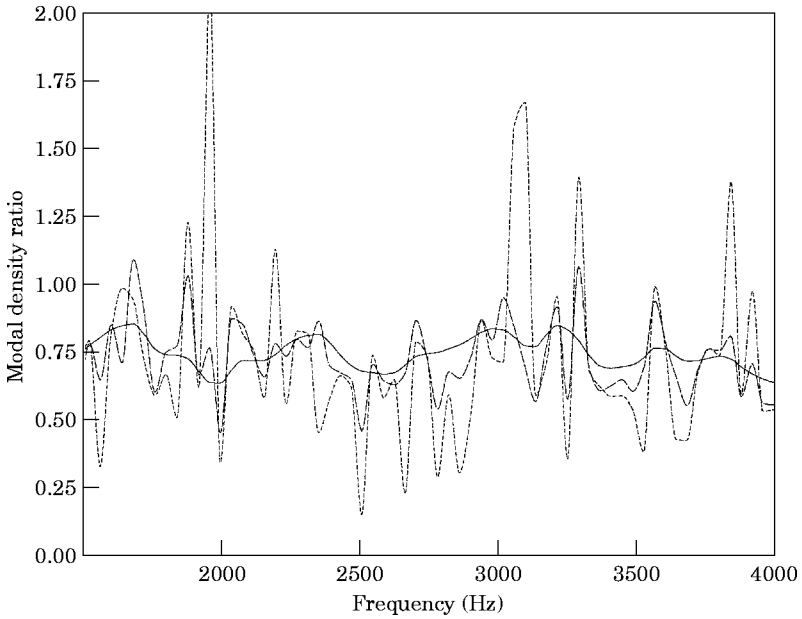

Figure 14. The influence of modal overlap factors on the apparent modal density ratio for example 3. ·····, MOF = 0·06; - - - - -, MOF = 1·0; ———, MOF = 6·0.

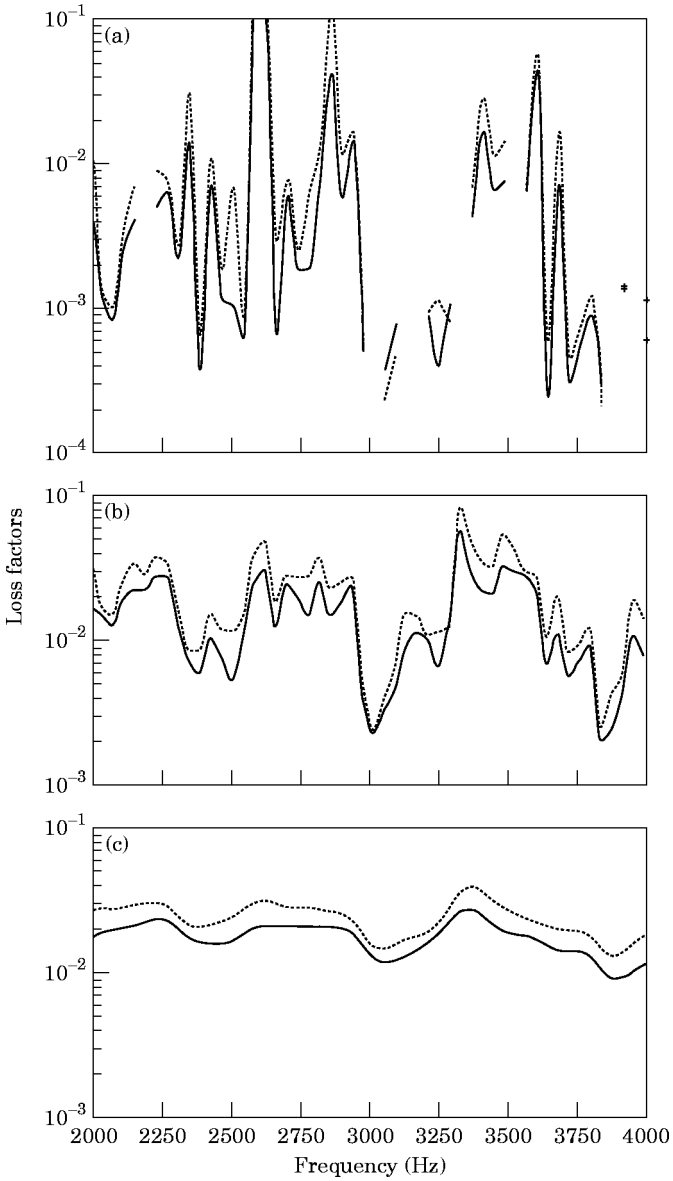

Figure 15. The influence of modal overlap factors on the coupling loss factors for example 3: (a) MOF = 0·06; (b) MOF = 1·0; (c) MOF = 6·0. Gaps in the curves indicate negative values, and + signs indicate discrete positive values. ———, η_{21}; - - - - -, η_{12}.

the results obtained from the FEA models in 500 Hz bands varied from 0·67 to 0·8, the average being 0·73.

It will be recalled that the MOF is the number of modes per Hz $\times$ $\eta\omega/2\pi$ and is therefore directly proportional to damping. Since there are about 0·03 and 0·04 modes per Hz for the two plates used, a damping coefficient ($c = \eta\omega$) of 200 s^{-1} gives approximately unit MOF in this case. The apparent modal density ratios and CLFs have therefore been calculated for three levels of damping leading to MOFs of approximately 0·06, 1·0 and 6·0 in both plates. In Figure 14 are shown the apparent modal density ratios, and their improvement at higher MOFs is apparent: the variations about the mean become less and

less. In this figure, the frequency averaged ratios calculated between 3000 and 4000 Hz (where the asymptotic value should apply) are 0·8, 0·7 and 0·73 for the three MOFs, respectively. It is thus clear that the mean value predicted for low MOF is rather greater than for plates with MOFs greater than unity, which are closer to the asymptotic value. In Figure 15 are shown the CLFs for these increasing values of MOF. It may be seen that at low MOFs and certain discrete frequencies, both of the CLFs are negative, such behaviour being also observed in reference [13], where it is suggested that this is due to non-reverberant energy transfer. Conversely, the CLFs are quite smooth at a MOF of 6·0. Note that the values of damping coefficients recovered from the CLF equations were always equal to the given values in these cases, since equations (6)–(9) can correctly model the energy flows at all MOFs and frequency ranges for this example, provided that negative CLFs are permitted. This is as expected, given that only two subsystems are involved and there are therefore no indirect CLFs to be dealt with.

5.2. EXAMPLE 4

The final example to be studied is a section taken from a ship (again see Figure 12). The complete model of the SWATH used to provide this section has approximately 34 000 degrees of freedom and 4700 elements [17]. The bulk of the elements in the model are of the quadrilateral plate, triangular plate and quadrilateral curved shell type. Lumped mass elements are used to model large masses of equipment. Beam elements are used either for non-structural items such as masts or stacks, or as plate stiffeners. The basic structure is stiffened by a large number of transverse bulkheads which connect the superstructure to the two hulls. Since the complete model of the ship was difficult to solve with the available computing facilities, due to its large size, the section taken from the aft portion was considered for study.

Here the two hulls are referred to as subsystems 1 and 3, and the superstructure as subsystems 2, as per Figure 16. This choice of subsystems is based on the rather obvious geometrical divisions in the structure; other breakdowns could, of course, be adopted and these might yield improved SEA models—such choices are often difficult to make in SEA work. In this case subsystems 1 and 3 each have 312 elements and 641 nodes. They are not completely identical, however, due to variations in the lumped mass models. Subsystem 2 has 591 elements and 1107 nodes and is not quite symmetrical.

For subsystems 1 and 3, 180 eigenvalues were extracted with four-digit accuracy in approximately four hours. These included six rigid body modes and spanned 80 Hz. For

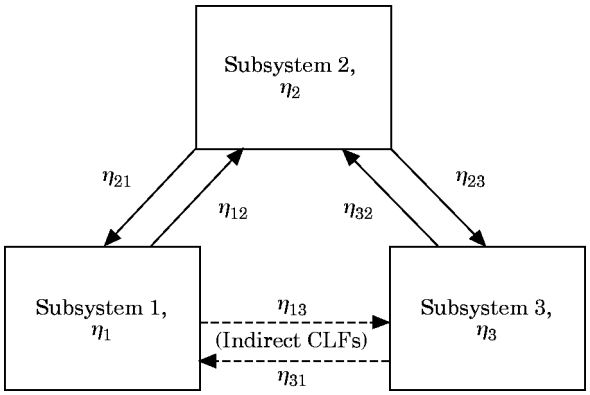

Figure 16. The subsystem model for the stern section of the SWATH ship of Example 4, showing SEA parameters.

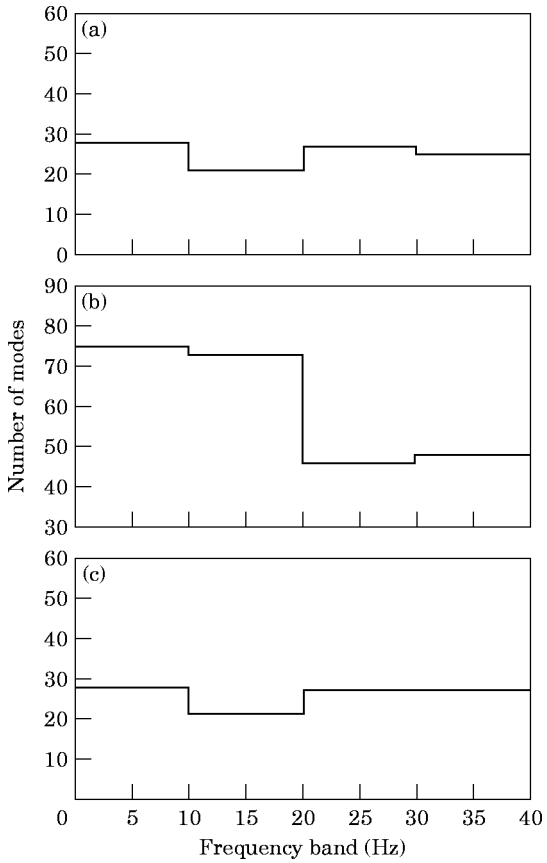

Figure 17. Variation of number of modes per 10 Hz frequency band with frequency for Example 4: (a) subsystem 1; (b) subsystem 2; (c) subsystem 3.

the much larger subsystem 2, the extraction of 266 eigenvalues with the same accuracy, but spanning just 50 Hz required around 18 hours. Given this upper limit for the second subsystem, only frequencies up to 40 Hz were studied when obtaining the CLFs. A global model of the aft section, combining subsystems 1, 2 and 3 and containing 2323 nodes, was also solved. Only 156 eigenvalues (spanning 7 Hz with three-digit accuracy) could be extracted for this model due to its large size, which even so took over 22 hours to deal with.

To carry out the receptance approach in this case, each frequency step in the solution required the assembly and solution of a 696×696 complex matrix, as 33 nodes (some having six and others five degrees of freedom) occur at each interface, this required about 10 minutes of CPU time per frequency. The CLFs to be studied in this example are also illustrated in Figure 16; they are calculated in the same manner as in the previous example; see equations (6)–(9). However, in this case, as there are three subsystems, it is possible to obtain nine equations for the cases corresponding to forcing subsystems 1, 2 and 3 alone in turn.

For this example, each subsystem was driven by harmonic forces applied at 25 randomly selected points. Averaging over 25 points was found to give marginally better results than attempts with 20 points and reflects the more complex subsystems being studied. In order to assure reasonable spatial distribution of the forces, each subsystem surface was divided

into four or five zones, with a fair sample being taken from each zone. The forces were chosen to be normal to the surface of application. The CLFs were evaluated for two different cases. First, all of the direct and indirect CLFs (η_{12}, η_{21}, η_{32}, η_{23}, η_{13}, η_{31}) together with the damping factors η_1, η_2, η_3 were evaluated. The values of the recalculated damping factors again as a check on the accuracy of the SEA equations. In the second case, the indirect CLFs were not considered in the equations: i.e., only seven unknowns were solved for, but again using nine equations. A minimal least squares solution method was used for solving the resulting sets of over-determined equations, allowing study of the effects of neglecting indirect CLFs in the SEA approach.

The distributions of modes for the three subsystems used in this study, in 10 Hz bands up to 40 Hz, are shown in Figure 17. It is seen that subsystems 1 and 3 have, on average, about 25 modes per band, whereas that of subsystem 2 varies significantly with frequency from about 75 to 50. The modal density ratio between the large and the small subsystems thus varies from 25/75 to 25/50: i.e., from about 0·3 to 0·5. In this case, MOFs exceeding unity are obtained by using damping coefficients of 10 s^{-1} and MOFs less than unity by using damping coefficients of 1 s^{-1}, for all three subsystems.

In Figure 18 is shown the variation of the direct and indirect CLFs with frequency, when the MOFs, are made much less than unity. It is clear that the CLFs are not well behaved and that negative values occur (where there are gaps in the logarithmic plots). In Figure 19 is shown the case in which the MOFs are made greater than unity: it is then possible to categorize the various CLFs, especially in the frequency ranges beyond 25 Hz; the two indirect CLFs have least values and lie at the bottom of the plot. They do, however, have negative values in some frequency ranges. Due to the near symmetry of the subsystems, it is to be expected that η_{12} and η_{32} should be similar, as should η_{21} and η_{23}, and here this is only approximately so, which seems to indicate the need for more thorough spatial averaging. This problem occurs because, in such complex FEA models, many of the

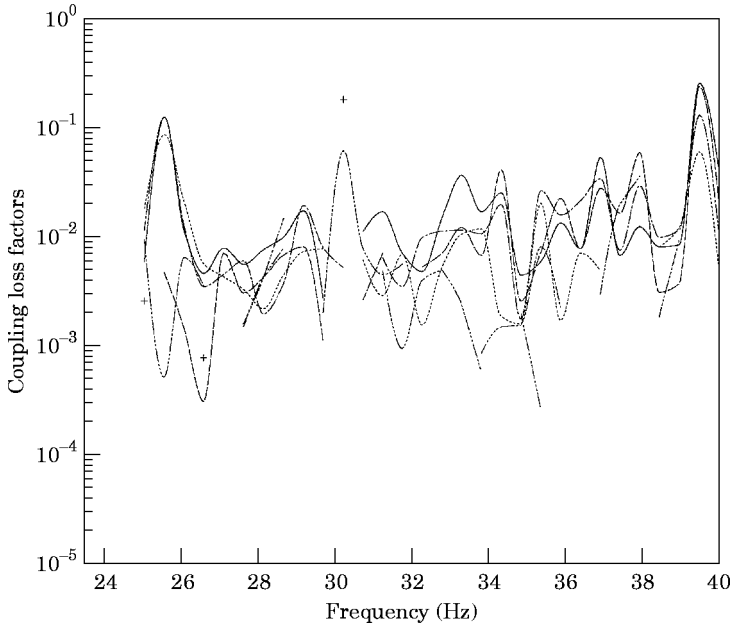

Figure 18. Variation of coupling loss factors with frequency for Example 4, with low modal overlap. Gaps in the curves indicate negative values, + signs indicate discrete positive values: ———, η_{12}; - - - - -, η_{21}; ....., η_{23}; —·—·—·—, η_{32}; —·····—·····—·····—, η_{13}; —···—···—, η_{31}.

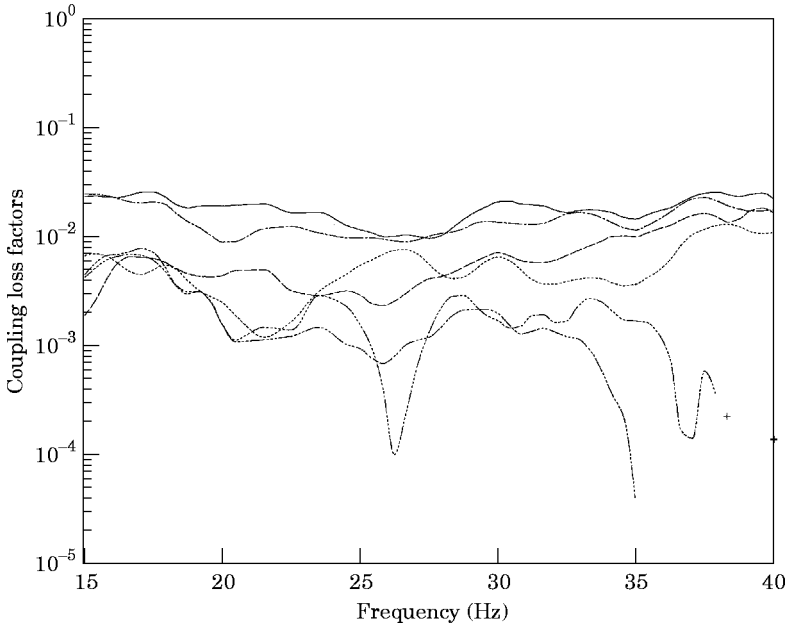

Figure 19. Variation of coupling loss factors with frequency for Example 4, with high modal overlap (key as Figure 18).

extracted mode shapes do not show significant responses throughout the domain being studied; such 'localized' modes are commonly encountered in large FEA analyses. The extracted values of the damping coefficients ($c_{1,2,3} = \eta_{1,2,3}\omega$) for both levels of damping again correctly match the given values, as expected, provided that negative and indirect CLFs are permitted.

Lastly, the frequency averaged CLFs in various 5 Hz bands are studied for the case in which $c_{1,2,3} = 10\ \mathrm{s}^{-1}$: i.e., at high MOF; see Tables 3 and 4. Here, averaging is carried out over 20 frequency points and again using 25 forcing points. For each band, results with

TABLE 3

Band averaged results obtained by using all CLFs (direct and indirect)

Band (Hz)	c_1	c_2	c_3	η_{12}	η_{21}	η_{32}	η_{23}	η_{31}	η_{13}	η_{21}/η_{12}	η_{23}/η_{32}
20–25	10	10	10	0·0172	0·00389	0·0111	0·00308	0·00121	0·00191	0·23	0·28
25–30	10	10	10	0·0131	0·00328	0·0112	0·00638	0·00171	0·00141	0·25	0·56
30–35	10	10	10	0·0186	0·00769	0·0142	0·00450	0·00105	0·00185	0·41	0·32
35–40	10	10	10	0·0213	0·0147	0·0178	0·00974	−0·00107	0·000347	0·69	0·55

TABLE 4

Band averaged results obtained by using only direct CLFs

Band (Hz)	c_1	c_2	c_3	η_{12}	η_{21}	η_{32}	η_{23}	η_{21}/η_{12}	η_{23}/η_{32}
20–25	10·3	9·9	10·2	0·0172	0·00401	0·0111	0·00337	0·23	0·30
25–30	10·3	9·8	10·3	0·0131	0·00407	0·0112	0·00683	0·31	0·61
30–35	10·6	8·2	10·5	0·0186	0·0112	0·0142	0·00961	0·60	0·68
35–40	9·9	10·4	9·8	0·0213	0·0127	0·0178	0·0101	0·60	0·57

and without indirect CLFs are plotted. The extracted damping coefficients c_1, c_2 and c_3 are also presented for comparison with the given value of 10 s^{-1}. It should be noted here that the 5 Hz bands contain more than ten modes in all cases; this was found necessary to gain reasonable results from applying the SEA equations, even at high modal overlap. This is in contrast to the often stated need for only five modes per band and is again related to the presence of localized modes in the FEA solutions.

A study of Tables 3 and 4 shows that inclusion of all the CLFs in the SEA equations gives correct results, since the damping values are accurately recovered. Notice that the indirect CLFs are smaller than the direct CLFs, although they are not entirely negligible. The recovered damping values obtained after neglecting the indirect CLFs show variations of 1% to 18% from the correct value, depending on the frequency band. This data shows that the contribution of indirect CLFs to the prediction of energy flows is quite significant in this case, despite the obvious geometrical split of the structure into three distinct pieces. In both cases the apparent modal density ratio η_{21}/η_{12} and η_{23}/η_{32} are representative of the actual values (which vary from 0·3 to 0·5 as mentioned previously), although they are not as similar as would be expected of a nearly symmetric structure. This again indicates the need for extensive sampling when evaluating spatial averages.

6. CONCLUSIONS

A method for predicting the energy flows between the subsystems of complex structures, by using receptance theory, has been presented. The subsystems are modelled as substructures by using a general purpose commercial FEA package, which are then solved separately for their mode shapes. The formulation is primarily intended for use in applications related to SEA, where information is required about subsystem energy levels and input powers and which is somewhat tedious to extract from global FEA models.

The method leads to a form of substructuring using free–free interface conditions which allows the direct evaluation of energy flows between the substructures. Additionally, and unlike modal synthesis methods, this approach can readily take into account variations in substructure damping. It is also possible to obtain exact results by including complete sets of substructure modes. Since the resulting matrix sizes are independent of the number of modes used, the problem of modal truncation in large models can easily be avoided. The examples presented clearly show that the reponse obtained by substructuring using a receptance formulation are identical to those from equivalent global models (which may span only a limited frequency domain due to modal truncation arising from limited computational resources) with appreciable saving in computational effort. It should be noted, however, that the size of the assembled Green function matrix depends on the number of coupling points between the substructures; hence it is desirable to define substructures with the minimum number of interface nodes. None the less, the method provides an efficient and accurate way of providing data for SEA studies.

This finite element substructure method has then been applied to energy flow studies for both simple and complex models, using an SEA-like framework. These examples are used to illustrate some of the advantages of this method over the conventional global model approach used in FEA: it makes higher frequency ranges accessible for a given computational effort; spatial averaging of external forcing is handled efficiently and it can handle different subsystem damping levels with no added complexity. The last two of these are of particular benefit in SEA work.

The simple plate model which is studied for the effects of varying modal overlap factors (MOFs) shows that these have a significant effect on the recovered coupling loss factors (CLFs). For the more complex marine vessel section, the indirect CLFs are found to be

smaller than the direct CLFs, especially at high MOFs, but even then they are by no means negligible, despite the obvious breakdown of the structure into three simply connected subsystems. Variation of the recovered internal damping coefficients as compared to the specified values is used as an indicator of the accuracy of the SEA solutions. As expected, the use of both negative and indirect CLFs in the SEA equations is found to yield these correctly for all frequencies and MOFs. Finally, the results for the larger structure indicate the spatial and frequency averaging needs to be carried out over many forcing points and modes to obtain good predictions of SEA parameters, because of the occurrence of many local modes in large FEA models.

REFERENCES

1. R. H. Lyon 1975 *Statistical Energy Analysis of Dynamical Systems*: *Theory and Applications*. Cambridge, MA: MIT Press.
2. K. Shankar and A. J. Keane 1995 *Journal of Sound and Vibration* **185**, 867–890. Energy flow predictions in a structure of rigidly joined beams using receptance theory.
3. R. E. D. Bishop and D. C. Johnson 1960 *The Mechanics of Vibration*. Cambridge: Cambridge University Press.
4. H. G. Davies 1972 *Journal of the Acoustical Society of America* **51**, 387–392. Exact solutions for the response of some coupled multimodal systems.
5. P. J. Remington and J. E. Manning 1975 *Journal of the Acoustical Society of America* **57**, 374–379. Comparison of statistical energy analysis power flow predictions with an 'exact' calculation.
6. B. L. Clarkson 1991 *Journal of Mechanical Engineering Science* (*Proceedings of the Institute of Mechanical Engineers*, *Part C*) **205**, 17–22, Estimation of the coupling loss factor of structural joints.
7. A. J. Keane and W. G. Price 1990 *Proceedings of the Institute of Acoustics* **12**, 535–542. Exact power flow relationships between many multi-coupled, multi-modal sub-systems.
8. D. J. Nefske and S. H. Sung 1989 *Journal of Vibration*, *Acoustics*, *Stress and Reliability in Design* **3**, 94–100. Power flow finite element analysis of dynamic systems: basic theory and application to beams.
9. P. C. Wood 1990 *Proceedings of the Institute of Acoustics* **12**, 571–578. The use of finite element methods in SEA applications.
10. S. A. Hambric 1990 *Journal of Vibration and Acoustics* **112**, 542–549. Power flow and mechanical intensity calculations in structural finite element analysis.
11. J. A. Steel and R. J. M. Craik 1994 *Journal of Sound and Vibration* **178**, 553–561. Statistical energy analysis of structure-borne sound-transmission by finite-element methods.
12. C. Simmons 1991 *Journal of Sound and Vibration* **144**, 215–227. Structure borne sound transmission through plate junction and estimates of SEA coupling loss factors using the Finite Element Method.
13. C. R. Fredo 1995 *Ph.D. Thesis*, *Chalmers Institute of Technology*, *Sweden*. A SEA-like approach for the derivation of energy flow coefficients with a finite element model.
14. Structural Dynamics Research Corporation 1993 *I-DEAS VI Reference Manual*. *S.D.R.C.*, OH, 45150, *U.S.A.*
15. A. J. Keane and W. G. Price 1987 *Journal of Sound and Vibration* **117**, 363–386. Statistical Energy Analysis of strongly coupled systems.
16. E. K. Dimitriadis and A. D. Pierce 1988 *Journal of Sound and Vibration* **123**, 497–412. Analytical solution for the power exchange between strongly coupled plates under random excitation: a test of Statistical Energy Analysis Concepts.
17. A. J. Keane, P. Temarel, X.-J. Wu and Y. S. Wu 1991 *Philosophical Transactions of the Royal Society of London* **A334**, 339–355. Hydroelasticity of non-beamlike ships in waves.